Probing Enzymatic PET Degradation: Molecular Dynamics Analysis of Cutinase Adsorption and Stability

Mehdi Sahihi, Pierre Fayon, Lionel Nauton, Florent Goujon, Julien Devémy, Alain Dequidt, Patrice Hauret, Patrice Malfreyt

Probing Enzymatic PET Degradation: Molecular Dynamics Analysis of Cutinase Adsorption and Stability

Mehdi Sahihi,*,† Pierre Fayon,‡ Lionel Nauton,† Florent Goujon,† Julien Devémy,† Alain Dequidt,† Patrice Hauret,¶ and Patrice Malfreyt*,†

†*Université Clermont Auvergne, Clermont Auvergne INP, CNRS, Institut de Chimie de Clermont-Ferrand, F-63000 Clermont-Ferrand, France*

‡*Université Clermont Auvergne, CHU Clermont Ferrand, Clermont Auvergne INP, CNRS, ICCF, F-63000 Clermont-Ferrand, France.*

¶*Manufacture Francaise des Pneumatiques Michelin, 23, Place des Carmes, 63040, Clermont-Ferrand, France*

E-mail: mehdi.sahihi@uca.fr; patrice.malfreyt@uca.fr

Abstract

Understanding the mechanisms influencing poly(ethylene terephthalate) (PET) biodegradation is crucial for developing innovative strategies to accelerate the breakdown of this persistent plastic. In this study, we employed all-atom molecular dynamics (MD) simulation to investigate the adsorption process of the LCC-ICCG cutinase enzyme onto the PET surface. Our results revealed that hydrophobic, π-π, and H-bond interactions, specifically involving aliphatic, aromatic, and polar uncharged amino acids, were the primary driving forces for the adsorption of the cutinase enzyme onto PET. Additionally, we observed a negligible change in the enzyme's tertiary structure during the interaction with PET (RMSD = 1.35 Å), while its secondary structures remained remarkably stable. Quantitative analysis further demonstrated that there is about 24% decrease in the number of the enzyme-water hydrogen bonds upon adsorption onto the PET surface.

The significance of this study lies in unraveling the molecular intricacies of the adsorption process, providing valuable insights into the initial steps of enzymatic PET degradation.

1 Introduction

Poly(ethylene terephthalate) (PET), produced from aromatic terephthalic acid (TPA) and ethylene glycol (EG), is a widely manufactured plastic, primarily employed in packaging (e.g., plastic bottles) and textile fibers. The global production of PET was projected to reach 87 million metric tons by the end of 2022.[1] After single-use, PET accumulates in the natural environment, with over 60% of PET waste ending up in landfills.[2] A significant quantity of microplastics is dispersed globally, even infiltrating pristine regions like the Arctic Polar Circle.[3] Furthermore, It is estimated that approximately 90% of all seabirds ingest plastic.[4] Despite the undeniable versatility of plastics in our daily lives, these findings underscore the pressing need to curb pollution through sustainable practices.[5]

One potential solution for mitigating PET waste involves recycling through mechanical[6] and chemical[7,8] degradation methods. However, these approaches come with certain limitations, including the requirement for high

temperatures, the generation of additional pollutants,[9] and the associated high reagent costs. Alternatively, biocatalytic degradation of PET offers an environmentally friendly solution for its recycling. While PET is generally considered challenging to biodegrade due to the presence of aromatic terephthalate units, various bacterial hydrolase enzymes, such as cutinases,[1,5,10–14] lipases,[15,16] carboxylesterases,[17,18] and esterases,[17,19] have been investigated for their ability to break down PET. However, PET hydrolase enzymes have shown limited productivity, posing a challenge for their application in the recycling industry.[20–22] Fortunately, recent advancements by Tournier et al.[13] have introduced modified ICCG and WCCG variants of the leaf-branch compost cutinase (LCC) as highly efficient and stable enzymes for PET biodegradation. Specifically, the LCC-ICCG protein, derived from LCC with mutations (F244I; D238C; S283C; Y127G), demonstrates remarkable capability, depolymerizing over 90% of PET into terephthalic acid (TPA) and ethylene glycol (EG) monomers within a mere 10-hour timeframe. LCC, is cloned from a fosmid library of a leaf-branch compost metagenome by functional screening using tributyrin agar plates, is overproduced in E. coli BL21-CodonPlus (DE3)-RP as a fusion protein with the pelB leader sequence and is purified from the extracellular medium.[23] Boneta et al.[24] suggested that the superior performance of the LCC-ICCG protein compared to PETase seems to stem from its ability to operate at elevated temperatures and its inherent connection with the crystallinity level of the polymer. Recent advancements in biocatalysis have opened new possibilities for efficient recycling of polyethylene terephthalate (PET). While this study primarily focuses on the enzymatic degradation of PET using LCC-ICCG, it is essential to acknowledge the broader landscape of promising candidates in this field. Notably, PHL7, as introduced by Sonnendecker et al.,[25] has emerged as a notable catalyst for PET degradation. Additionally, Richter et al.[26] have presented variants of PHL7 with enhanced catalytic activities. These variants offer exciting prospects for advancing the field of biocatalytic PET recycling. However, our preliminary molecular docking studies shows the higher affinity of LCC-ICCG variant compared to more recent introduced variants of LCC (Table S1) highlighting the importance of this variant for more detailed investigations.

The bio-depolymerization (bio-degradation) of PET is indeed a complex process that necessitates the investigation of different phenomena and the determination of various properties. These include: i) Thermodynamic characterization of the PET-water interfacial region; ii) The adsorption process of the enzyme onto the PET surface; and iii) The binding mode between PET and the catalytic site of the enzyme. To address these intricate processes and properties, molecular simulation emerges as a valuable method. It allows for an adapted description of interactions, tailored to the specific process and properties under investigation. In the case of the PET-water interface, atomistic simulations have been conducted to predict the work of adhesion between water and the amorphous PET surface.[27] These simulations provide insights into the strength of interactions between these two media. Additionally, the free energy cost associated with extracting a monomer from PET material in various environments, including water, dodecane, ethylene glycol, and vacuum have been assessed. Intriguingly, the results indicate that such extractions were energetically unfavorable across all considered conditions. Also, to tackle the reaction mechanism occurring within the active pocket, researchers often employ a multi-scale hybrid approach, such as Quantum Mechanics/Molecular Mechanics (QM/MM).[24,28–30]

While there have been several published computational studies on the molecular mechanism of cutinase enzyme degradation of PET,[31–33] there remains a notable absence of a comprehensive investigation that delves into all the aforementioned processes involved in this degradation with molecular and atomic-level details. For example, the adsorption procedure of the enzyme onto the PET surface and starting point of the enzymatic reaction have not been investigated, yet. Exploring the adsorption process of a protein[34,35] onto the surface of

a polymeric material presents a formidable challenge for molecular methods. This is primarily attributed to the large system size, the heterogeneous nature of the adsorption surface, the structural flexibility of the adsorbate, and the consequently lengthy simulation time required for system relaxation. Nevertheless, recent advancements have made it possible to investigate the properties of an adsorbed enzyme on a surface over extended periods, spanning tens of nanoseconds.[14,36–39]

The present study aims to address the biodepolymerization of PET in a holistic manner, filling the existing gap in understanding of different phenomena and the determination of various properties of PET bio-degradation. Building upon a comprehensive investigation of the PET-water interface[27] to assess the strength of interactions between water and PET, as well as the energy costs associated with extracting PET monomers in various solvents, this work focuses on probing the adsorption of the LCC-ICCG enzyme onto the PET surface. The adsorption process is elucidated by calculating the interaction energy and examining changes in the enzyme's structural and hydration properties compared to bulk water conditions. Our MD simulation serves as a robust tool for probing the molecular events at the interface between cutinase enzyme and PET. This comprehensive approach enhances our understanding of the enzymatic degradation of PET, contributing to the development of eco-friendly strategies for plastic waste management and represents a pivotal stride toward a more environmentally conscious and sustainable future.

2 Computational procedure

The simulated system comprises a cutinase enzyme suspended in a water droplet, initially positioned in proximity to a PET surface. The cutinase enzyme, composed of 258 amino acid residues, was sourced from the RCSB protein data bank (PDB ID: 6THT; see Figure 1). This structure, obtained through X-ray diffraction methods, was originally reported by Tournier et al.[13] with a resolution of 1.14 Å and an R-value of 0.137. The enzyme's structure encompasses 3,848 atoms and carries a total charge of +6 e at pH = 7. Prior to employing the coordinates from the crystallographic structure in the MD simulation procedure, the determination of missing side chains and the protonation state of histidine residues was carried out using the WHATIF web interface.[40] To prepare the simulation system, we utilized the "gmx editconf" and "gmx solvate" modules from GROMACS[41–44] for solvating the enzyme structure within a cubic box. Subsequently, all solvent molecules beyond a 10 Å solvation shell were removed using Visual Molecular Dynamics (VMD). By simulating the enzyme in a water droplet, we can capture essential aspects of the enzyme adsorption process while maintaining computational efficiency. The system was neutralized by introducing Sodium and Chloride ions at a concentration of 150 mM. This process added an additional 3129 water molecules to solvate the cutinase enzyme. All molecular dynamics (MD) simulations were conducted using the GROMACS 2021.6 simulation package.[41–44] The CHARMM36 force field, previously validated for studying protein-polymer interactions,[38] was employed for all simulations. Additionally, we used the TIP3P water model, as included in CHARMM36, for our simulations. The enzyme-in-water system underwent energy minimization and equilibration in an NVT ensemble for a duration of 1 ns.

We employed the GaussView[45] and Gaussian16[46] software to prepare and optimize the structure of a 9-mer chain of PET, utilizing the PM6 semi-empirical method. This choice strikes a balance between computational feasibility and capturing essential features of amorphous PET, including commonly observed polymer length in amorphous PET materials.[47] While we acknowledge that real PET chains can be longer, the selected chain length allows for an in-depth exploration of key interactions and dynamic behavior within our computational model. Subsequently, we constructed a PET slab with dimensions measuring $10 \times 10 \times 5\,\mathrm{nm}^3$, comprising a total of 231 PET chains. The resulting PET density is approx-

imately 1.29 g cm^{-3}, closely mirroring the reported experimental value of 1.34 g cm^{-3} for amorphous PET[48] and validating the representation of our computational model against reported densities.

The PET chains were parameterized using the CHARMM36 force field, as depicted in Figure S2 and summarized in Table S2. This force field has previously demonstrated successful utility in constructing PET samples.[49,50]

To initiate the simulations, the initial structure of PET underwent energy minimization and equilibration over 1 ns within an NVT ensemble. To create the amorphous form of the PET slab, the equilibrated PET chains underwent a heating-cooling procedure (300 K-1000 K-300 K) at a rate of 50 K ns^{-1}. To accurately model the PET slab assembly in our molecular dynamics simulations, we considered the conformational distribution of the OC–CO ethylene glycol torsion angle. It is noteworthy that our analysis revealed that, in our model, all polymer chains predominantly exhibit a gauche conformation for the OC–CO ethylene glycol torsion angle (Figure S3). This stands in contrast to the reported 1:10 trans-to-gauche ratio observed in amorphous PET.[51] While we acknowledge the importance of accurately representing the conformational distribution in amorphous PET, we would like to emphasize that our primary focus in this study is the interaction of the enzyme with the surface of the polymer.

Then, the system was centered within a cubic box, with a total of 58,998 atoms for the composite system consisting of the PET slab, a water droplet containing a cutinase enzyme, and sodium and chloride ions. The enzyme's active site was positioned atop the PET slab, with the distance between the water droplet and PET set at approximately 5.0 Å (see Figure 1). In parallel, we also prepared a system involving only the enzyme in water, without the polymer slab.

The integration of equations of motion was conducted using a time step of 1.0 fs while employing XY periodic boundary conditions (PBC). To prevent the undesired diffusion of water molecules in the Z-direction, we introduced an implicit repulsive wall, represented by a 10-4 Lennard-Jones potential, at the top of the simulation box for the enzyme-PET complex. The systems underwent an energy minimization process using the Conjugate Gradient (CG) method, with convergence criteria set at 1×10^{-6} kJ mol^{-1} for energy difference and 1×10^{-6} kJ mol^{-1} nm^{-1} for RMS force. Subsequently, three 0.5 µs replicate NVT production runs were performed at 338 K (an optimized temperature for the catalytic activity of the cutinase enzyme[13]). Temperature was raised from 300 K to 338 K at a rate of 5 K ns^{-1} (using a Nose-Hoover thermostat[52] with a damping constant of 0.2 ps). A 1.0 nm cutoff was employed for Lennard-Jones and Coulomb interactions. Additionally, we utilized the particle mesh-Ewald (PME) method[53,54] and the LINCS algorithm[55] for handling long-range electrostatics and constraints, respectively.

3 Results and Discussion

3.1 Cutinase adsorption onto the PET surface

As we observe the time evolution trajectory at a temperature of 338 K, a pivotal aspect of the simulation becomes apparent: the interaction between the enzyme and the surface of the PET slab initiates at approximately 70 ps. This interaction is primarily instigated by the Tyr95 amino acid residue within the enzyme's active pocket. It is worth noting that the minimum distance between this residue and the PET chains at this stage measures approximately 0.35 nm, underscoring the significance of π-π stacking interactions in catalyzing the interaction between the cutinase enzyme and the PET slab (refer to Figure 2a). Around the 2 ns mark, in addition to various aromatic residues of the protein, uncharged and aliphatic amino acid residues also engage with the polymer's surface, thereby further stabilizing the system. During this phase, a PET polymer chain is attracted towards the enzyme's binding pocket, establishing interactions with the Tyr95, Trp190, and Met166 amino acid residues, which have

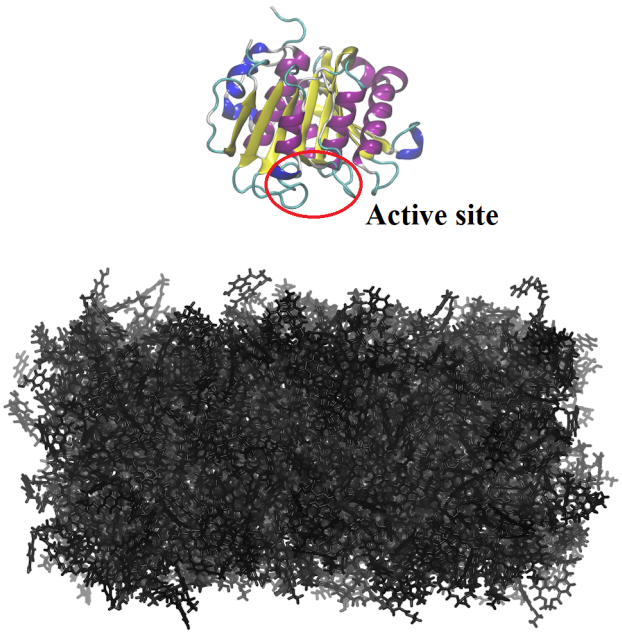

Figure 1: The side view of the constructed system for MD simulation of the cutinase enzyme (PDB ID:6THT) adsorption onto the PET surface. The size of PET slab is $10 \times 10 \times 5\,\mathrm{nm}^3$ and the water molecules are not shown for more clear view.

been identified as crucial elements in initiating the enzymatic reaction[13] (as depicted in Figure 2b). Subsequently, the protein undergoes spatial conformational adjustments, forming more extensive contacts with the surface. It attains a relatively stable state at approximately 150 ns, maintaining this stable state until the conclusion of the simulation (see Figures 2c and 2d). This dynamic evolution, from the initial interaction to stable adhesion and conformational adjustments, sheds light on the intricate interplay between the cutinase enzyme and the PET substrate, offering valuable insights into the enzymatic process.

We have undertaken a comprehensive quantitative analysis of the interaction dynamics between the cutinase enzyme and the PET surface. All the quantities for the enzyme-PET surface were averaged over all three replicate MD simulations. Figure S1 illustrates the overlay of the final protein configurations obtained from three independent replicates of MD simulations. Our initial focus centers on discerning the spatial distribution and the local environment of the cutinase by quantifying the number of hydrogen bonds established between the enzyme, water molecules, and the PET surface. To ensure robust statistical analysis, we have considered the last 350 ns of the simulation, during which the protein reaches a stable state. In Figure 3a, we present an overview of the number of each amino acid in contact with water and positioned within the inner part of the enzyme as it interfaces with the PET surface. The enzyme's orientation is strategically designed so that its most hydrophilic residues maintain direct contact with water. It is notable that a significant proportion of Ser, Arg, Asn, and Asp residues are situated within a distance of less than 0.35 nm from the water, indicating their potential to establish persistent hydrogen bonds with the surrounding aqueous environment. In contrast, amino acid residues characterized by uncharged and aliphatic side chains, indicative of hydrophobic interactions, predominate among those in contact with the PET surface. Additionally, π-π interactions between the PET substrate and aromatic residues such as Phe, Tyr, and Trp play a crucial role in stabilizing the cutinase-PET complex. It is essential to highlight that the total number of residues in contact with water is 190, whereas

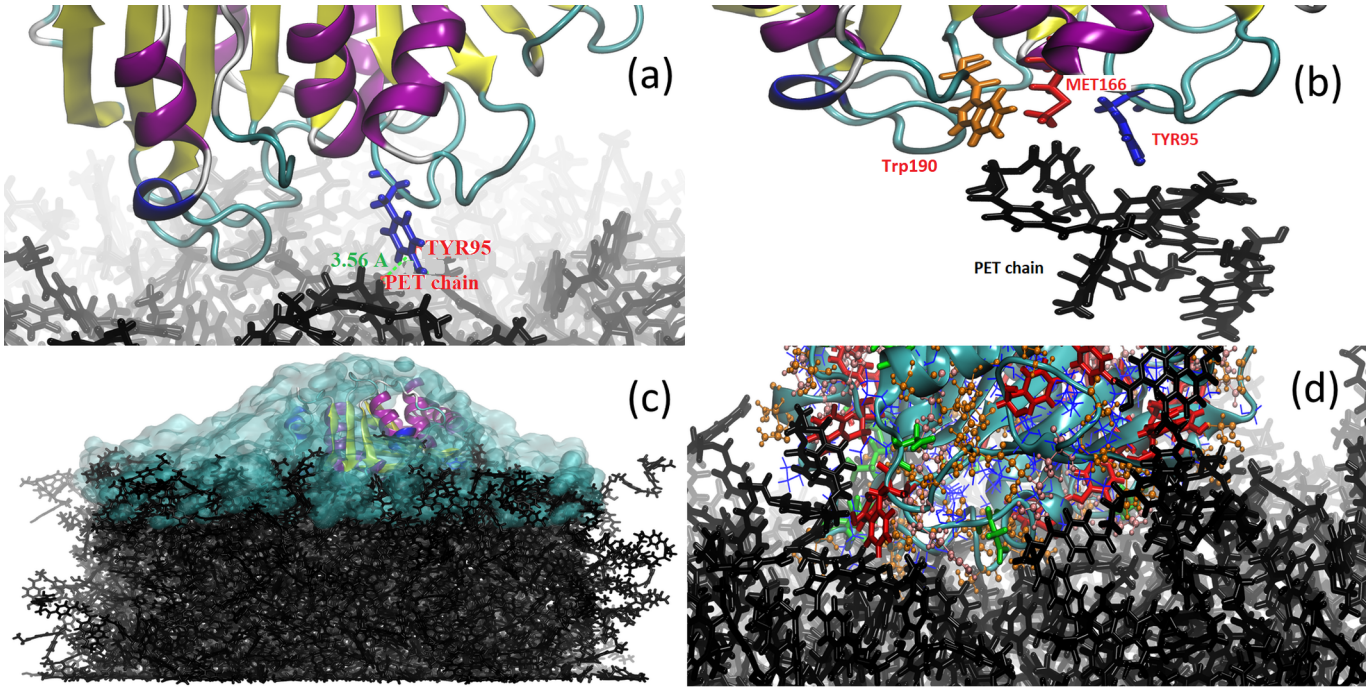

Figure 2: Representative snapshots of the MD simulation of the cutinase enzyme adsorbed onto the surface of a PET slab (a) 70 ps; the π-π interaction between TYR95 and the PET chains (TYR95 amino acid residue is shown by blue licorice representation), (b) 2 ns; moving a PET chain toward the enzyme's active pocket and interacting with its amino acid residues, (c) 0.5 µs; final configuration of the cutinase enzyme on the surface of PET, and (d) different types of amino acid residues which are interacting with the surface of PET polymer during the last 350 ns of simulation trajectory (aliphatic, aromatic, polar uncharged, acidic and basic amino acid residues are shown by blue line, red bond, orange CPK, green licorice and pink CPK representations, respectively).

in a pure water environment, this number increases to 205. The disparity between these two counts can be attributed to the residues directly interfacing with the PET surface. Importantly, this number remains constant throughout the final 350 ns of the simulation, rendering this timeframe a robust choice for the acquisition of average values and yielding a valuable criterion for analysis.

The analysis reveals that, on average, the cutinase establishes a total of 243 hydrogen bonds when adsorbed onto the PET surface, while this number increases to 312 in a pure water environment. This 24% decrease in the number of hydrogen bonds upon adsorption highlights the significant displacement of solvent molecules, which can be observed in Figure 2c. Figure 3b presents the number of hydrogen bonds between each residue of the cutinase and both water molecules and the PET surface. As anticipated, the most hydrophilic residues exhibit the highest contribution to the formation of hydrogen bonds and are less likely to engage in interactions with the hydrophobic PET surface. The majority of these residues serve as hydrogen bond acceptors, with the exceptions being Ser and Arg. Remarkably, only seven hydrogen bonds are established between the enzyme and the PET surface. Given that these interactions involve the same residues throughout the simulation, we can deduce that the enzyme is effectively immobilized on the PET surface.

We delved into the structural aspects of the cutinase-PET complex by scrutinizing the density profile along the z-axis, perpendicular to the surface, as elucidated in Figure 4a. To isolate the structure from the influence of the surrounding water molecules, we considered only the atoms within a range of 0.8 nm of the enzyme's center of mass, projected onto the xy plane. This range was thoughtfully chosen to be narrower than the xy component of the en-

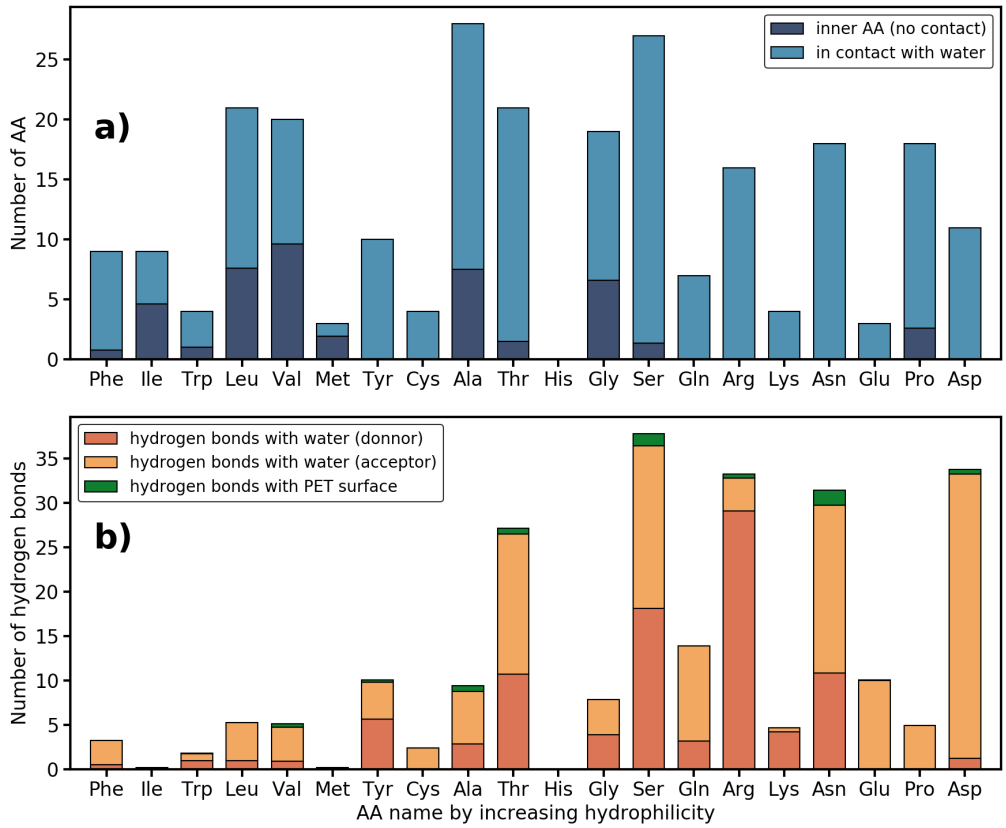

Figure 3: (a) average number of each amino acid in contact with water and in the inner part of the cutinase when adsorbed onto the PET surface, (b) average number of hydrogen bonds done by each amino acid by the adsorbed cutinase.

zyme's radius of gyration, allowing us to exclude most of the surrounding solvent while retaining sufficient statistical data.

The analysis reveals that the enzyme prominently maintains direct contact with the PET surface, with only a minimal presence of water molecules at the interface. Furthermore, the residues comprising the active pocket site, as depicted in Figure 2b, are positioned in proximity to the surface. Notably, the density peak in the profile is quite sharp, indicating that both the active pocket site and the enzyme itself are robustly immobilized on the PET surface during the data acquisition phase. Figure 4b provides a snapshot that exemplifies water-mediated hydrogen bond interactions that contribute to the stabilization of the cutinase enzyme on the PET surface. Indeed, the adsorbed configuration entails shared hydration water molecules bridging interactions between the cutinase enzyme and the PET chains. Consequently, it can be inferred that the primary driving forces underpinning the enzyme's adsorption onto the PET surface encompass hydrophobic interactions, hydrogen bonds, and π-π interactions.

To further explore the alteration in the environment of the active pocket site once the enzyme is adsorbed onto the surface, we performed an analysis by calculating the radial distribution function between the center of mass of the active site and the neighboring water molecules, as illustrated in Figure 5. This analysis provides insights into how the local interaction dynamics within the active pocket change upon enzyme adsorption to the PET surface.

The observed peak at 0.65 nm in the radial distribution function signifies a distinct alteration in the distribution of water molecules in the enzyme's active site as enzyme adsorbs onto the PET surface and a PET chain sticks inside its active pocket. This modification is

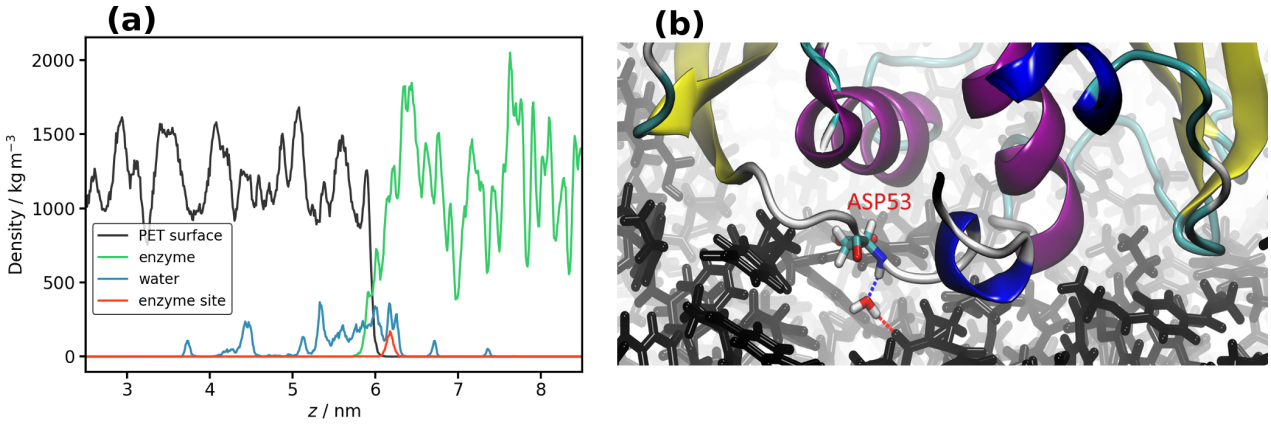

Figure 4: (a) average density profile of each molecular type close to the active pocket during the last 350 ns of the MD simulation trajectory; (b) an example of water-mediated H-bond interaction between Asp53 amino acid residue and PET.

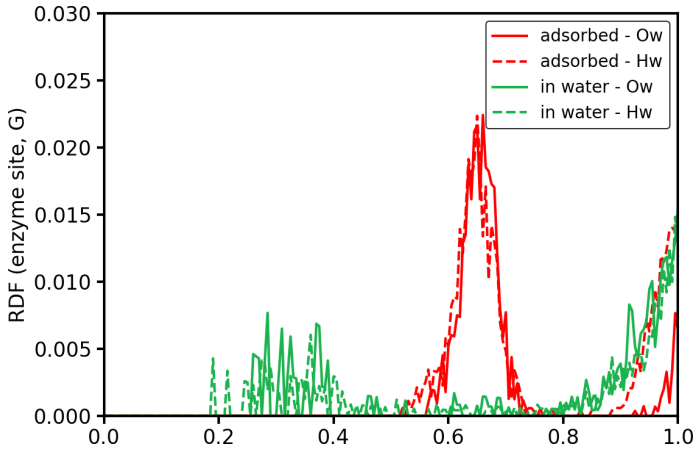

Figure 5: radial distribution function of water atoms (Ow and Hw) calculated from the center of mass of the enzyme active site, for the adsorbed enzyme and the enzyme in water. To ensure robust statistical analysis, we have considered the last 350 ns of the simulation, during which the protein reaches a stable state.

attributed to the inclusion of water molecules closer to the center of the active pocket. Notably, this specific peak is absent when the enzyme is analyzed in a pure water environment.

The presence of this peak suggests that the adsorption of the enzyme onto a surface, in this case, the PET surface, leads to a specific reconfiguration of the pocket site. This reconfiguration arises from the changes in the local environment surrounding the active site. These alterations in the geometry and the proximity of water molecules within the active pocket may, in turn, impact the reactivity of the pocket, potentially allowing it to exhibit a specific behavior or reactivity unique to its environment when adsorbed on the PET surface. This dynamic response of the active site to its environment is a key aspect of the enzyme's functionality and interaction with its substrate.

Figure S4 represents the trend of interaction energy with the evolution of time that is totally consistent with the contact details discussed before. When the enzyme was adsorbed onto the PET surface, the interaction energy decreased. Other considerable changes were observed at about 350 ns and remained stable at about -631.91 ± 44.34, -308.24 ± 68.86, and -940.14 ± 85.72 kJ mol^{-1}, for LJ, coulomb and total energy, respectively.

3.2 Conformational changes

To gain insights into the overall shape and orientation of the enzyme in relation to the surface, we conducted an analysis by calculating the radius of gyration (Rg) tensor of the enzyme. The eigenvalues of this tensor, denoted as λ_1, λ_2 and λ_3 correspond to the components of the Rg in the molecule frame. In simpler terms, they represent the radii of the ellipsoid that characterizes the molecule's shape. Figure 6a depicts the time evolution of these three eigenvalues for the enzyme in a water environment and when adsorbed onto the PET surface. In a slightly oblate geometry, two larger eigenvalues and one smaller eigenvalue are typical.

While the Rg components exhibit significant fluctuations in pure water, all three eigenvalues remain relatively constant during the acquisition phase when the enzyme is adsorbed onto the PET surface. The reduced fluctuations in the case of the adsorbed enzyme suggest that its conformation becomes more stable in the presence of the surface. The most notable change in shape upon enzyme adsorption is evident in the smallest eigenvalue, λ_3 (0.789 nm in water, 0.752 nm when adsorbed), signifying a slight and negligible flattening of the enzyme as it adheres to the PET surface. The orientation of the enzyme is further investigated by considering the three eigenvalues as the orientations of the primary axes of the enzyme, denoted as $\mathbf{v}_1$, $\mathbf{v}_2$ and $\mathbf{v}_3$. Figure 6b illustrates the time evolution of the angles between these main axes and the normal vector (n) to the surface, which corresponds to the z-axis. The analysis reveals that the enzyme's orientation undergoes very small changes during the initial 50 ns but subsequently stabilizes into two axes aligned parallel to the surface and the third axis aligned perpendicular to the surface. This stable orientation underscores the enzyme's firm adhesion to the PET surface, facilitated by a combination of hydrophobic, hydrogen bond, and π-π interactions.

To delve deeper into the conformational changes of the enzyme, we conducted an analysis of its backbone Root Mean Square Deviation (RMSD) relative to the crystal structure. As depicted in Figure 6c, the RMSD for the simulated systems exhibits an initial increase with time, ultimately reaching equilibrium values after approximately 350 and 150 ns for enzyme in water and adsorbed enzyme, respectively. Furthermore, when comparing the changes in RMSD between both systems, namely the cutinase in a water environment and the cutinase-PET complex, a notable observation emerges. The interaction of the enzyme with PET significantly stabilizes its structure and leads to fewer conformational changes in its 3D configuration.

We employed the residue-based Root-Mean-Square Fluctuation (RMSF) analysis, based on the average positions of amino acid residues, to assess their local dynamic variations. This approach enables us to identify regions within the protein that undergo significant structural changes and fluctuations during the simulation. This analysis was done at the last 150 ns of MD simulation trajectories to be sure that both of the systems are behaving as equilibrated systems. In Figure 6d, we observe that when cutinase is adsorbed onto the PET surface, the amino acid residues experience greater stability, resulting in reduced fluctuations when compared to the cutinase in a water environment. Notably, amino acid residues that engage in interactions with the PET surface, such as SER67 and ALA224, or those positioned within the active site of the enzyme, like TYR95, which interacts with a PET chain, display lower RMSF values in contrast to their counterparts in the free cutinase. This observation suggests that the interaction of PET with the enzyme's amino acid residues mitigates their flexibility, leading to increased stabilization. Consequently, the enzyme's adsorption onto the PET surface imparts a greater degree of structural rigidity to these critical amino acid residues. Similar behavior has been previously reported about the interaction of PETase and PET dimer.[56]

In our comprehensive analysis, we also examined the secondary structure of the cutinase enzyme using the DSSP module[57] of Gromacs. It is evident from the results that the secondary structures of the enzyme remain remarkably stable throughout the entire duration of the MD simulation, as indicated in Table 1. This sta-

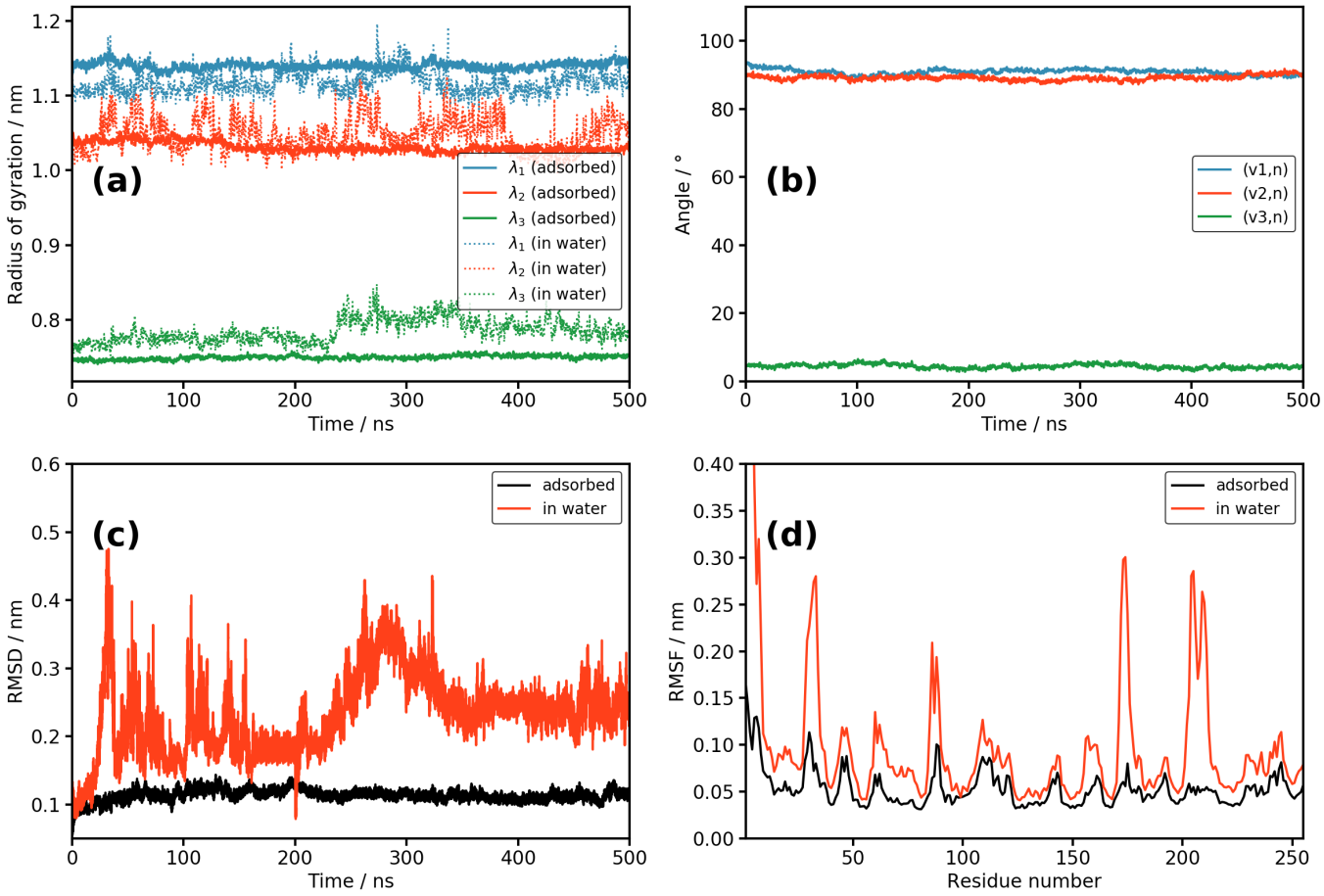

Figure 6: (a) The three eigenvalues of the gyration tensor of the enzyme as a function of time. The full lines and dotted lines represent the enzyme adsorbed onto the PET surface and the enzyme in water, respectively. (b) The angle between the normal to the surface **n** and the eigenvectors of the gyration tensor of the adsorbed enzyme as a function of time. (c) RMSD of all backbone carbon atoms of cutinase in enzyme-PET and enzyme in water systems. (d) root-mean-square fluctuation (RMSF) of cutinase amino acid residues in enzyme-PET and enzyme in water systems during the last 150 ns of MD simulation trajectories.

bility underscores a significant finding: during the interaction of cutinase with PET, the enzyme undergoes a small and negligible tertiary structural changes and the stability of its secondary structures is preserved. This remarkable feature highlights the enzyme's capacity to maintain its key structural components while engaging with the PET substrate, underlining its efficiency in catalyzing reactions involving PET. We conducted a more detailed analysis and incorporated Figure S5. The overlay of the initial and final configurations clearly illustrates that the tertiary conformational changes are indeed negligible. This observation aligns with our findings from the RMSD analysis, where the overall structural changes are approximately 1.35 Å. These data support our assertion that, while present, the tertiary structural changes are subtle and consistent with the enzyme's ability to maintain stability in its secondary structures.

4 Conclusions

In conclusion, our study leveraged all-atom MD simulations to provide a comprehensive analysis of the recently introduced LCC-ICCG cutinase enzyme onto the PET surface. Our investigation delved into the molecular, atomic, ener-

Table 1: Changes in the Secondary Structure of cutinase due to Its adsorption onto the PET Surface

Type of Secondary Structure	Initial percentage	Final percentage
Coil	21.70 ± 1.15	23.26 ± 1.18
β-Sheet	23.26 ± 1.18	22.61 ± 1.12
β-Bridge	0	0
Bend	11.63 ± 0.61	11.76 ± 0.59
Turn	14.73 ± 0.78	10.98 ± 0.58
α-Helix	26.36 ± 1.21	25.84 ± 1.36
5-Helix	0	0
3-Helix	2.32 ± 0.12	5.56 ± 0.24

getic, and mechanistic details of the adsorption process of the cutinase enzyme onto the PET surface.

Analysis of the trajectory for the cutinase-PET system revealed several key insights. Firstly, the interaction between the enzyme and PET initiates rapidly during the initial stages of the MD simulation. This interaction is primarily stabilized by a combination of hydrophobic, hydrogen bond, and π-π interactions between the PET chains and hydrophobic, polar-uncharged, and aromatic amino acid residues of the cutinase enzyme. Interfacial water molecules also play a pivotal role in facilitating these interactions. Comparing the trajectories of the cutinase-PET and cutinase in water systems demonstrated that the tertiary structure of the enzyme undergoes slight and negligible changes during its interaction with PET, and the secondary structures remain stable. Moreover, amino acid residues that interact with the PET surface exhibit reduced flexibility compared to other amino acids, underscoring the robust interaction between cutinase and PET. Interestingly, our findings indicate that the presence of the cutinase enzyme in the environment makes it easier to extract a PET monomer into water.

In summary, our study contributes valuable insights into the intricate molecular and mechanistic aspects of the LCC-ICCG cutinase enzyme adsorption on PET, shedding light on the complex interplay of interactions that is considered as starting point of this catalytic process.

Acknowledgement This work was performed in SimatLab, a joint public-private laboratory dedicated to the multi-scale modelling of polymer materials. This laboratory is supported by Michelin, Clermont Auvergne University (UCA), CHU of Clermont-Ferrand and CNRS. We are also grateful to the Mesocenter Clermont Auvergne University for providing computing and storage resources.

Supporting Information Available

Atoms types in the CHARMM force field, description of the PET monomer, protonated terminal residues, distribution of dihedral angles, interaction energy changes during the adsorption process, and overlay of enzyme conformations during the adsorption process.

Data and Software Availability statement

The cutinase enzyme, composed of 258 amino acid residues, was sourced from the RCSB protein data bank (PDB ID: 6THT). We employed the GaussView (https://gaussian.com/gaussview6) and Gaussian16 (https://gaussian.com/gaussian16) software to prepare and optimize the structure of a 9-mer chain of PET. Specific open source software from third parties was also used: GROMACS version 2021.6 (https://www.manual.gromacs.org/documentation/2021.6/download.html/), VMD1.9 (http://www.ks.uiuc.edu/Research/vmd/),and WHATIF web interface (https://swift.cmbi.umcn.nl/servers/html/index.html). Input and output files are available at https://zenodo.org/doi/10.5281/zenodo.10374812 (and also from the corresponding author upon request).

References

(1) Urbanek, A. K.; Kosiorowska, K. E.; Mirończuk, A. M. Current Knowledge

on Polyethylene Terephthalate Degradation by Genetically Modified Microorganisms. *Front. Bioeng. Biotechnol.* **2021**, *9*, 771133.

(2) Koshti, R.; Mehta, L.; Samarth, N. Biological Recycling of Polyethylene Terephthalate: A Mini-Review. *J. Polym. Environ.* **2018**, *26*, 3520–3529.

(3) Cozar, A.; Marti, E.; Duarte, C. M.; de Lomas, J. G.; Sebille, E. V.; Ballatore, T. J.; Eguiluz, V. M.; Gonzales-Gordillo, J. I.; Pedrotti, M. L.; Echevarria, F.; Trouble, R.; Irigoien, X. The Arctic Ocean as a Dead End for Floating Plastics in the North Atlantic branch of the Thermohaline Circulation. *Sci. Adv.* **2017**, *3*, e1600582.

(4) Wilcox, C.; Sebille, E. V.; Hardesty, B. D. Threat of Plastic Pollution to Seabirds Is Global, Pervasive, and Increasing. *Proc. Natl. Acad. Sci. USA* **2015**, *112*, 11899–11904.

(5) Furukawa, M.; Kawakami, N.; Tomizawa, A.; Miyamoto, K. Efficient degradation of poly (ethylene terephthalate) with Thermobifida fusca cutinase exhibiting improved catalytic activity generated using mutagenesis and additive-based approaches. *Sci. Rep* **2019**, *9*, 16038.

(6) Park, S. H.; Kim, S. H. Poly (ethylene terephthalate) Recycling for High Value Added Textiles. *Fashion Text.* **2014**, *1*, 1.

(7) Imran, M.; Kim, D. H.; Al-Masry, W. A.; Mahmood, A.; Hassan, A.; Haider, S.; Ramay, S. M. Manganese-, Cobalt-, and Zinc-Based Mixed-Oxide Spinels as Novel Catalysts for the Chemical Recycling of Poly(ethylene Terephthalate) via Glycolysis. *Polym. Degrad. Stab.* **2013**, *98*, 904–915.

(8) Liu, Y.; Yao, X.; Yao, H.; Zhou, Q.; Xin, J.; Lu, X.; Zhang, S. Degradation of Poly(ethylene Terephthalate) Catalyzed by Metal-free Choline-Based Ionic Liquids. *Green Chem.* **2020**, *22*, 3122–3131.

(9) Marshall, I.; Todd, A. The Thermal Degradation of Polyethylene Terephthalate. *Trans. Faraday Soc.* **1953**, *49*, 67–68.

(10) Brueckner, T.; Eberl, A.; Heumann, S.; Rabe, M.; Guebitz, G. M. Enzymatic and chemical hydrolysis of poly (ethylene terephthalate) fabrics. *J. Polym. Sci. A* **2008**, *46*, 6435–6443.

(11) Yoshida, S.; Hiraga, K.; Takehana, T.; Taniguchi, I.; Yamaji, H.; Maeda, Y.; Toyohara, K.; Miyamoto, K.; Kimura, Y.; Oda, K. A bacterium that degrades and assimilates poly (ethylene terephthalate). *Science* **2016**, *351*, 1196–1199.

(12) Wei, R.; Breite, D.; Song, C.; Gräsing, D.; Ploss, T.; Hille, P.; Schwerdtfeger, R.; Matysik, J.; Schulze, A.; Zimmermann, W. Biocatalytic degradation efficiency of postconsumer polyethylene terephthalate packaging determined by their polymer microstructures. *Adv. Sci.* **2019**, *6*, 1900491.

(13) Tournier, V.; Topham, C.; Gilles, A.; David, B.; Folgoas, C.; Moya-Leclair, E.; Kamionka, E.; Desrousseaux, M.-L.; Texier, H.; Gavalda, S.; Cot, M.; Guémard, E.; Dalibey, M.; Nomme, J.; Cioci, G.; Barbe, S.; Chateau, M.; André, I.; Duquesne, S.; Marty, A. An engineered PET depolymerase to break down and recycle plastic bottles. *Nature* **2020**, *580*, 216–219.

(14) Pfaff, L.; Gao, J.; Li, Z.; Jäckering, A.; Weber, G.; Mican, J.; Chen, Y.; Dong, W.; Han, X.; Feiler, C. G.; znd Christoffel P.S. Badenhorst, Y.-F. A.; Bednar, D.; Palm, G. J.; Lammers, M.; Damborsky, J.; Strodel, B.; Liu, W.; Bornscheuer, U. T.; Wei, R. Multiple Substrate Binding Mode-Guided Engineering of a Thermophilic PET Hydrolase. *ACS Catal.* **2022**, *12*, 9790–9800.

(15) Vertommen, M.; Nierstrasz, V.; Van Der Veer, M.; Warmoeskerken, M. Enzymatic surface modification of poly (ethylene terephthalate). *J. Biotechnol.* **2005**, *120*, 376–386.

(16) Mueller, R.-J. Biological degradation of synthetic polyesters—Enzymes as potential catalysts for polyester recycling. *Process Biochem.* **2006**, *41*, 2124–2128.

(17) Barth, M.; Honak, A.; Oeser, T.; Wei, R.; Belisário-Ferrari, M. R.; Then, J.; Schmidt, J.; Zimmermann, W. A dual enzyme system composed of a polyester hydrolase and a carboxylesterase enhances the biocatalytic degradation of polyethylene terephthalate films. *Biotechnol. J.* **2016**, *11*, 1082–1087.

(18) Ghodke, V. M.; Punekar, N. S. Environmental role of aromatic carboxylesterases. *Environ. Microbiol.* **2022**, *24*, 2657–2668.

(19) Barzkar, N.; Sohail, M.; Tamadoni Jahromi, S.; Gozari, M.; Poormozaffar, S.; Nahavandi, R.; Hafezieh, M. Marine bacterial esterases: Emerging biocatalysts for industrial applications. *Appl. Biochem. Biotechnol.* **2021**, *193*, 1187–1214.

(20) de Castro, A. M.; Carniel, A.; Nicomedes Junior, J.; da Conceição Gomes, A.; Valoni, É. Screening of commercial enzymes for poly (ethylene terephthalate)(PET) hydrolysis and synergy studies on different substrate sources. *J. Int. Microbiol. Biotechnol.* **2017**, *44*, 835–844.

(21) Wei, R.; Zimmermann, W. Biocatalysis as a green route for recycling the recalcitrant plastic polyethylene terephthalate. *Microb. Biotechnol.* **2017**, *10*, 1302.

(22) Kawai, F.; Kawabata, T.; Oda, M. Current knowledge on enzymatic PET degradation and its possible application to waste stream management and other fields. *Appl. Microbiol. Biotechnol.* **2019**, *103*, 4253–4268.

(23) Sulaiman, S.; Yamato, S.; Kanaya, E.; Kim, J.-J.; Koga, Y.; Takano, K.; Kanaya, S. Isolation of a novel cutinase homolog with polyethylene terephthalate-degrading activity from leaf-branch compost by using a metagenomic approach. *Appl. Environ. Microbiol.* **2012**, *78*, 1556–1562.

(24) Boneta, S.; Arafet, K.; Moliner, V. QM/MM Study of the Enzymatic Biodegradation Mechanism of Polyethylene Terephthalate. *J. Chem. Inf. Model.* **2021**, *61*, 3041–3051.

(25) Sonnendecker, C.; Oeser, J.; Richter, P. K.; Hille, P.; Zhao, Z.; Fischer, C.; Lippold, H.; Blázquez-Sánchez, P.; Engelberger, F.; Ramírez-Sarmiento, C. A.; Oeser, T.; Lihanova, Y.; Frank, R.; Jahnke, H.-G.; Billig, S.; Abel, B.; Sträter, N.; Matysik, J.; Zimmermann, W. Low carbon footprint recycling of post-consumer PET plastic with a metagenomic polyester hydrolase. *ChemSusChem* **2022**, *15*, e202101062.

(26) Richter, P. K.; Blázquez-Sánchez, P.; Zhao, Z.; Engelberger, F.; Wiebeler, C.; Künze, G.; Frank, R.; Krinke, D.; Frezzotti, E.; Lihanova, Y.; Falkenstein, P.; Matysik, J.; Zimmermann, W.; Sträter, N.; Sonnendecker, C. Structure and function of the metagenomic plastic-degrading polyester hydrolase PHL7 bound to its product. *Nat. Commun.* **2023**, *14*, 1905.

(27) Fayon, P.; Devémy, J.; Emeriau-Viard, C.; Ballerat-Busserolles, K.; Goujon, F.; Dequidt, A.; Marty, A.; Hauret, P.; Malfreyt, P. Energetic and Structural Characterizations of the PET-Water Interface as a Key-step in Understanding its Depolymerization. *J. Phys. Chem. B* **2023**, *127*, 3543–3555.

(28) Warshel, A.; Levitt, M. Theoretical Studies of Enzymatic Reactions: Dielectric, Electrostatic and Steric Stabilization of the Carbonium Ion in The Reaction of

Lysozyme. *J. Mol. Biol.* **1976**, *103*, 227–249.

(29) Knott, B. C.; Erickson, E.; Allen, M. D.; Gado, J. E.; Graham, R.; Kearns, F. L.; Pardo, I.; Topuzlu, E.; Anderson, J. J.; Austin, H. P.; Dominick, G.; Johnson, C. W.; Rorrer, N. A.; Szostkiewicz, C. J.; Copié, V.; Payne, C. M.; Woodcock, H. L.; Donohoe, B. S.; Beckham, G. T.; McGeehan, J. E. Characterization and engineering of a two-enzyme system for plastics depolymerization. *Proc. Natl. Acad. Sci. U.S.A.* **2020**, *117*, 25476–25485.

(30) Pinto, A. V.; Ferreira, P.; Neves, R. P.; Fernandes, P. A.; Ramos, M. J.; Magalhaes, A. L. Reaction mechanism of MHETase, a PET degrading enzyme. *ACS Catal.* **2021**, *11*, 10416–10428.

(31) Li, Q.; Zheng, Y.; Su, T.; Wang, Q.; Liang, Q.; Zhang, Z.; Qi, Q.; Tian, J. Computational design of a cutinase for plastic biodegradation by mining molecular dynamics simulations trajectories. *Comput. Struct. Biotechnol. J.* **2022**, *20*, 459–470.

(32) Groß, C.; Hamacher, K.; Schmitz, K.; Jager, S. Cleavage product accumulation decreases the activity of cutinase during PET hydrolysis. *J. Chem. Inf. Model.* **2017**, *57*, 243–255.

(33) Aboelnga, M. M.; Kalyaanamoorthy, S. QM/MM Investigation to Identify the Hallmarks of Superior PET Biodegradation Activity of PETase over Cutinase. *ACS Sustain. Chem. Eng.* **2022**, *10*, 15857–15868.

(34) Zhang, L.; Sun, Y. Molecular Simulation of Adsorption and its Implications to Protein Chromatography: A Review. *Biochem. Eng. J.* **2010**, *48*, 408–415.

(35) Dalkas, G.; Euston, S. R. Molecular Simulation of Protein Adsorption and Conformation at Gas-Liquid, Liquid–Liquid and Solid–Liquid Interfaces. *Curr. Opin. Colloid Interface Sci.* **2019**, *41*, 1–10.

(36) Branco, R. J.; Graber, M.; Denis, V.; Pleiss, J. Molecular mechanism of the hydration of Candida antarctica lipase B in the gas phase: Water adsorption isotherms and molecular dynamics simulations. *Chembiochem* **2009**, *10*, 2913–2919.

(37) Zhao, D.; Peng, C.; Zhou, J. Lipase adsorption on different nanomaterials: a multi-scale simulation study. *Phys. Chem. Chem. Phys.* **2015**, *17*, 840–850.

(38) Sahihi, M.; Faraudo, J. Molecular Dynamics Simulations of Adsorption of SARS-CoV-2 Spike Protein on Polystyrene Surface. *J. Chem. Inf. Model.* **2022**, *62*, 3814–3824.

(39) Sahihi, M.; Faraudo, J. Computer Simulation of the interaction between SARS-CoV-2 Spike Protein and the Surface of Coinage Metals. *Langmuir* **2022**, *38*, 14673–14685.

(40) Vriend, G. WHAT IF: a molecular modeling and drug design program. *J. Mol. Graph.* **1990**, *8*, 52–56.

(41) Berendsen, H. J.; van der Spoel, D.; van Drunen, R. GROMACS: A message-passing parallel molecular dynamics implementation. *Comput. Phys. Commun.* **1995**, *91*, 43–56.

(42) Lindahl, E.; Hess, B.; Van Der Spoel, D. GROMACS 3.0: a package for molecular simulation and trajectory analysis. *J. Mol. Model.* **2001**, *7*, 306–317.

(43) Berendsen, H.; Hess, B.; Lindahl, E.; Van Der Spoel, D.; Mark, A.; Groenhof, G. GROMACS: fast, flexible, and free. *J. Comput. Chem* **2005**, *26*, 1701–1718.

(44) Abraham, M. J.; Murtola, T.; Schulz, R.; Páll, S.; Smith, J. C.; Hess, B.; Lindahl, E. GROMACS: High performance molecular simulations through multi-level parallelism from laptops to supercomputers. *Softwarex* **2015**, *1*, 19–25.

(45) Dennington, R.; Keith, T. A.; Millam, J. M. GaussView Version 6. 2019; Semichem Inc. Shawnee Mission KS.

(46) Frisch, M. J.; Trucks, G. W.; Schlegel, H. B.; Scuseria, G. E.; Robb, M. A.; Cheeseman, J. R.; Scalmani, G.; Barone, V.; Petersson, G. A.; Nakatsuji, H.; Li, X.; Caricato, M.; Marenich, A. V.; Bloino, J.; Janesko, B. G.; Gomperts, R.; Mennucci, B.; Hratchian, H. P.; Ortiz, J. V.; Izmaylov, A. F.; Sonnenberg, J. L.; Williams-Young, D.; Ding, F.; Lipparini, F.; Egidi, F.; Goings, J.; Peng, B.; Petrone, A.; Henderson, T.; Ranasinghe, D.; Zakrzewski, V. G.; Gao, J.; Rega, N.; Zheng, G.; Liang, W.; Hada, M.; Ehara, M.; Toyota, K.; Fukuda, R.; Hasegawa, J.; Ishida, M.; Nakajima, T.; Honda, Y.; Kitao, O.; Nakai, H.; Vreven, T.; Throssell, K.; Montgomery, J. A., Jr.; Peralta, J. E.; Ogliaro, F.; Bearpark, M. J.; Heyd, J. J.; Brothers, E. N.; Kudin, K. N.; Staroverov, V. N.; Keith, T. A.; Kobayashi, R.; Normand, J.; Raghavachari, K.; Rendell, A. P.; Burant, J. C.; Iyengar, S. S.; Tomasi, J.; Cossi, M.; Millam, J. M.; Klene, M.; Adamo, C.; Cammi, R.; Ochterski, J. W.; Martin, R. L.; Morokuma, K.; Farkas, O.; Foresman, J. B.; Fox, D. J. Gaussian˜16 Revision C.01. 2016; Gaussian Inc. Wallingford CT.

(47) Roberge, M.; Prud'homme, R. E.; Brisson, J. Molecular modelling of the uniaxial deformation of amorphous polyethylene terephthalate. *Polymer* **2004**, *45*, 1401–1411.

(48) Thompson, A.; Woods, D. Density of amorphous polyethylene terephthalate. *Nature* **1955**, *176*, 78–79.

(49) Shen, W.; Wang, X.; Zhang, G.; Kluth, P.; Wang, Y.; Liu, F. Illustrating the atomic structure and formation mechanism of ion tracks in polyethylene terephthalate with molecular dynamics simulations. *Nucl. Instrum. Methods Phys. Res., Sect. B* **2023**, *535*, 102–111.

(50) Cruz-Chu, E. R.; Ritz, T.; Siwy, Z. S.; Schulten, K. Molecular control of ionic conduction in polymer nanopores. *Faraday Discuss.* **2009**, *143*, 47–62.

(51) Wei, R.; Song, C.; Gräsing, D.; Schneider, T.; Bielytskyi, P.; Böttcher, D.; Matysik, J.; Bornscheuer, U. T.; Zimmermann, W. Conformational fitting of a flexible oligomeric substrate does not explain the enzymatic PET degradation. *Nat. Commun.* **2019**, *10*, 5581.

(52) Evans, D. J.; Holian, B. L. The nose–hoover thermostat. *J. Chem. Phys.* **1985**, *83*, 4069–4074.

(53) Essmann, U.; Perera, L.; Berkowitz, M. L.; Darden, T.; Lee, H.; Pedersen, L. G. A smooth particle mesh Ewald method. *J. Chem. Phys.* **1995**, *103*, 8577–8593.

(54) Darden, T.; York, D.; Pedersen, L. Particle mesh Ewald: An N log (N) method for Ewald sums in large systems. *J. Chem. Phys.* **1993**, *98*, 10089–10092.

(55) Hess, B.; Bekker, H.; Berendsen, H. J.; Fraaije, J. G. LINCS: A linear constraint solver for molecular simulations. *J. Comput. Chem.* **1997**, *18*, 1463–1472.

(56) Fecker, T.; Galaz-Davison, P.; Engelberger, F.; Narui, Y.; Sotomayor, M.; Parra, L. P.; Ramírez-Sarmiento, C. A. Active site flexibility as a hallmark for efficient PET degradation by I. sakaiensis PETase. *Biophys. J.* **2018**, *114*, 1302–1312.

(57) Touw, W. G.; Baakman, C.; Black, J.; Te Beek, T. A.; Krieger, E.; Joosten, R. P.; Vriend, G. A series of PDB-related databanks for everyday needs. *Nucleic Acids Res.* **2015**, *43*, D364–D368.

TOC Graphic